

Relationships between Molecular Properties and Biological Activities of *O*-Phenyl Pyrrolidino- and Piperidinocarbamate Herbicides

Ujjana B. Nandihalli,[†] Mary V. Duke, and Stephen O. Duke*

Southern Weed Science Laboratory, Agricultural Research Service, U.S. Department of Agriculture,
P.O. Box 350, Stoneville, Mississippi 38776

The molecular properties of phenopylate (2,4-dichlorophenyl 1-pyrrolidinecarboxylate) and 13 of its *O*-phenyl pyrrolidino- and piperidinocarbamate analogues were correlated with their capacity to inhibit protoporphyrinogen oxidase (Protox), to cause accumulation of protoporphyrin IX, and to cause herbicidal injury. All three biological properties correlated well with the van der Waals volume, electrophilic superdelocalizability, and energy of the lowest unoccupied molecular orbital. The relationships between biological activities and log *P* were curvilinear. The activity was mainly centered on the phenyl ring. Highly active molecules carry atoms or groups on the phenyl ring that generate at least two negative electrostatic potential fields located opposite each other. We suggest that these electrostatic fields are involved in the initial recognition by the receptor as well as in the noncovalent interaction with the enzyme binding site, possibly by hydrogen bonding. The substitutions on the phenyl ring may also be essential for optimal steric fit into the receptor cleft. In competitive binding studies utilizing unlabeled phenopylate and its analogues to compete [¹⁴C]acifluorfen off of etioplast membranes, the phenopylate analogues were found to bind to the same sites on Protox as acifluorfen, a competitive inhibitor which is suggested to mimic two adjacent pyrrole rings of protoporphyrinogen IX.

INTRODUCTION

Photobleaching herbicides from several different chemical classes, including certain oxadiazoles, diphenyl ethers, pyrazole phenyl ethers, and *N*-phenylimides, are potent inhibitors of protoporphyrinogen oxidase (Protox) (Matringe et al., 1989a,b; Witkowski and Halling, 1989; Jacobs et al., 1990, 1991; Sherman et al., 1991a,b; Camadro et al., 1991). Protox is the last enzyme common to the synthesis of both heme and chlorophyll. Inhibition of Protox leads to accumulation of high concentrations of protoporphyrin IX (Proto IX) (Matringe and Scalla, 1988a,b; Lydon and Duke, 1988; Witkowski and Halling, 1988; Becerril and Duke, 1989; Nicolaus et al., 1989; Matsumoto and Duke, 1990; Nandihalli et al., 1991). Apparently, when Protox is inhibited, protoporphyrinogen (Protogen), its substrate, leaves the chloroplast and is rapidly oxidized outside the normal porphyrin pathway to Proto IX (Jacobs et al., 1991; Lehnen et al., 1990). Proto IX accumulates in or near the plasmalemma and, in the presence of molecular oxygen and light, generates highly destructive singlet oxygen (Duke et al., 1990, 1991). The process is similar to the accumulation and cellular damage in humans and yeast with genetic defects in Protox (Deybach et al., 1981; Camadro et al., 1982).

We have recently shown that phenopylate and 13 of its analogues (*O*-phenyl pyrrolidino- and piperidinocarbamates) (Table I) inhibit Protox, induce Proto IX accumulation, and cause herbicidal damage in barley (*Hordeum vulgare* L.) and cucumber (*Cucumis sativus* L.) (Nandihalli et al., 1992b). There was a close relationship between all three of these parameters. Among 24 Protox-inhibiting diphenyl ethers there was poor correlation among these traits (Nandihalli et al., 1992a). However, certain molecular properties of diphenyl ethers did correlate with each biological parameter. In this paper, we demonstrate

that phenopylate and its analogues bind to the same site as acifluorfen on etioplast membranes and we present quantitative and qualitative relationships between semiempirical molecular properties and biochemical and biological activities of phenopylate and its analogues.

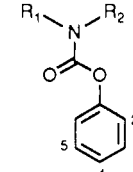
MATERIALS AND METHODS

Biochemical and Biological Activities. The data of Protox inhibition, Proto IX accumulation, and herbicidal activity of the 14 analogues were taken from our previous work (Nandihalli et al., 1992b). The Protox inhibition was represented by I_{50} , which is the concentration of the herbicide required to reduce the enzyme activity by 50% and is expressed as log I_{50} in the regression equation. Similarly, log Proto IX is that log of the amount of protoporphyrin IX caused to accumulate by 100 μ M herbicide. Herbicidal activity (HA) was evaluated by measuring electrolyte leakage from herbicide-treated tissue into the external medium.

Binding Studies. The procedures for growing barley plants and isolating etioplasts have been described previously (Sherman et al., 1991a,b). The procedure of Tischer and Strotmann (1977) was used to determine binding of [¹⁴C]acifluorfen (AF) to barley etioplasts in the presence or absence of selected phenopylate analogues. Etioplasts (0.6 mg of protein) were suspended in a reaction solution consisting of 0.33 M sorbitol, 0.1 M 2-[4-(2-hydroxyethyl)piperazin-1-yl]ethanesulfonic acid (HEPES), 1 mM ethylenediaminetetraacetic acid (EDTA), and 1 mM MgCl₂, and solution pH was maintained at 7.7 using HEPES buffer. Various concentrations (2–100 nM) of [¹⁴C]-labeled AF (specific activity of 18.03 mCi/mmol, uniformly ring labeled) plus 100 nM of each of selected phenopylate analogues were added. The suspensions were thoroughly mixed and incubated for 30 min on ice. The samples were centrifuged for 6 min at 12000g at 4 °C. The supernatant was transferred to vials and mixed with 12 mL of premixed scintillation cocktail (Aquasol) for radioactivity measurements. The inner walls of tubes were wiped dry with cotton swabs without disturbing the pellets to remove any adhering [¹⁴C]. A 100- μ L aliquot of tissue solubilizer (Protosol) was added to pellets and heated in a water bath at 50 °C for 15 min. The slurry was transferred to vials, and 10 mL of Aquasol was added for radioactivity measurements. The amount of [¹⁴C]AF bound was calculated from the radioactivity in pellets. The concentrations added were taken as free AF. Specific binding constants were estimated from double-reciprocal plots of bound AF vs free

* Author to whom correspondence should be addressed.

[†] Permanent address: Hazelton Laboratories, 3301 Kinsman Blvd., Madison, WI 53707.

Table I. Structures and Protox I_{50} Values of Compounds Used in the Study


no.	compd	2	4	5	R ₁	R ₂	I_{50} , μM
1	RH-1908	H	H	H	—(CH ₂) ₄ —		4000
2	RH-1909	Cl	H	H	—(CH ₂) ₄ —		240
3	RH-1911	H	Cl	H	—(CH ₂) ₄ —		11.5
4	RH-7160	Cl	Cl	OCH ₂ C≡CH	C ₂ H ₅	C ₂ H ₅	7.5
5	RH-9611	Cl	Cl	OH	—(CH ₂) ₄ —		4.7
6	phenopylate	Cl	Cl	H	—(CH ₂) ₄ —		2.7
7	RH-1965	Cl	Cl	CO ₂ CH ₃	—(CH ₂) ₄ —		0.7
8	RH-1964	Cl	Cl	CO ₂ <i>i</i> -Pr	—(CH ₂) ₄ —		0.4
9	RH-6251	Cl	Cl	OCH ₂ C≡CH	—(CH ₂) ₅ —		0.28
10	RH-0710	Cl	—OCH ₂ CO(CH ₂ C≡CH)N—		—(CH ₂) ₄ —		0.15
11	RH-4663	Cl	Cl	OCH ₂ C≡CH	—(CH ₂) ₄ —		0.12
12	RH-1224	Cl	Cl	—OCH ₂ C≡CH	—(CH ₂) ₂ CF ₂ (CH ₂) ₂ —		0.045
13	RH-0978	Cl	Cl	—OCH ₂ C≡CH	—(CH ₂) ₂ CF ₂ CH ₂ —		0.030
14	RH-1422	F	Cl	CO ₂ <i>i</i> -Pr	—(CH ₂) ₄ —		0.021

Table II. List of Semiempirical Molecular Descriptors Used in QSAR Analysis

type	descriptors
whole molecule properties	
bulk descriptors	van der Waals volume (VDW _{volume}) van der Waals area (VDW _{area})
shape descriptors	maximum lengths of <i>x</i> , <i>y</i> , and <i>z</i> axes
electronic descriptors	dipole moment molecular electrostatic potentials + and - volumes and area (+MEP _{volume} , -MEP _{volume} , +MEP _{area} , and -MEP _{area}) superdelocalizability (<i>S</i>) <i>S</i> _{HOMO} , <i>S</i> _{LUMO} , electrophile <i>S</i> (<i>S</i> _E), and nucleophile <i>S</i> (<i>S</i> _N)
energy descriptors	energy of HOMO (ϵ_{HOMO}) and LUMO (ϵ_{LUMO})
lipophilicity descriptor	log <i>P</i>
atom-centered electronic properties	partial charge, <i>S</i> _E , and <i>S</i> _N of six carbon atoms of the phenyl ring

AF (Tischer and Strotmann, 1977). For example, extrapolation of AF alone regression plot in Figure 2 to the *x* axis gave a value of 0.02432 1/nM or 41.1 nM which is the specific binding constant of AF (Figure 2).

Estimation of Partition Coefficients. Reversed-phase high-performance liquid chromatography (RP-HPLC) was used for estimating partition coefficients (*P*) of 14 nonionic herbicides used in the study (Ellgehausen et al., 1981). This technique involved determination of capacity factors (*K'*) for compounds with a wide range of known partition coefficients and development of a standard curve of log *P* vs log *K'*. Using the same RP-HPLC conditions as used in the standard curve, the capacity factors for herbicides were determined. The log *P* of herbicides was calculated using the linear regression equation of the form log *P* = *a* + *b* (log *K'*). The HPLC system was composed of Waters Associates components which included Model 510 pumps; a Model 712 autosampler, a Maxima 820 controller, and a Model 990 photodiode array detector. The column was a 250 × 4.6 mm (i.d.) Spherisorb 5- μm ODS-1 reversed-phase column. The mobile phase was methanol/water (75:25 v/v) at a flow rate of 1.4 mL/min. The column temperature was maintained at 28 °C by a Waters temperature control and column heater module. The injection volume was 5 μL . The detector was set at 254 nm.

Molecular Properties. We used the Chem-X (Chemical Design Limited, Oxford, U.K.) molecular modeling software for computing various molecular properties (Table II) of phenopylate analogues.

Selection of Model Structure. Since there were no 3D crystal structures available for any of the analogues in the study, we selected an analogue which showed the highest intrinsic inhibitory activity at the enzyme site as a template upon which the molecular

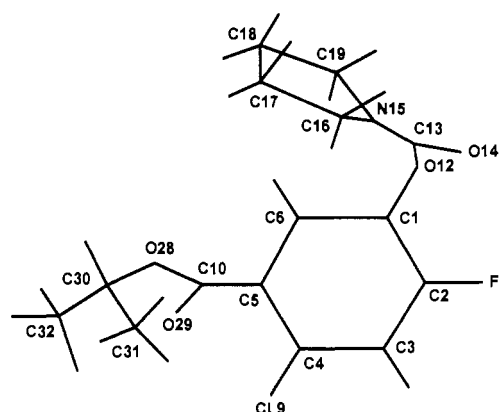


Figure 1. Optimized structure of RH-1422. Hydrogen atoms are not labeled.

properties of other analogues could be based. RH-1422 had the highest Protox-inhibiting activity with relatively greater Proto IX inducing and herbicidal capacities. The 3D structure of RH-1422 was built using the standard atoms and fragments available in the molecular mechanics parameter file of the Chem-X software. Empirical parameters were used for setting bond lengths and angles during structure building.

Conformational Analysis and Geometry Optimization. Since RH-1422 is a flexible molecule, a conformational search for locating the minimum energy conformer(s) was undertaken. We used four rotatable bonds (N15—C13, C13—O12, O12—C1, and C5—C10) in the structure (Figure 1) as search variables and rotated over 360° in 30° increments. These four bonds were selected because these were the only common rotatable bonds to most of the analogues in the set. The lowest energy conformer was then subjected to full geometry optimization via MOPAC (Quantum Chemistry Exchange Program 560, version 6.0, Department of Chemistry, Indiana University, Bloomington, IN) using modified neglect of diatomic overlap (MNDO) parameterization. Ground electronic states were obtained as closed-shell molecular orbital wave functions in the restricted Hartree-Fock framework.

The structures of other analogues in the study were built on the optimized structure of RH-1422 (Figure 1). These structures were also optimized for geometry as above. Each analogue was fitted to optimized structure of RH-1422 before its molecular properties were calculated.

Calculation of 3D Maps. The van der Waals (VDW) volume maps were calculated using Chem-X, which displays the surface of the molecule at the VDW radius. To map VDW volume (VDW_{volume}) using contour, Chem-X uses a continuous function, instead of a step function, for describing the transition across the molecular surface. The volume enclosed by a contour level of 1 was computed by multiplying the total number of grid points

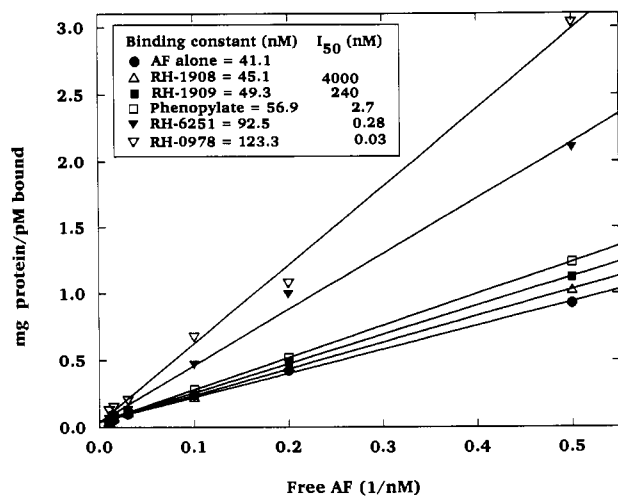


Figure 2. Binding of labeled acifluorfen (AF) in the presence of 100 nM unlabeled phenopylate and its analogues.

in the display lattice which lie inside the contour by the separation between the grid points along each axis of the lattice.

The molecular electrostatic potential (MEP) is the interaction energy of a point positive unit charge with the atoms of the structure. Chem-X treats the charge on each atom in a molecule as a point charge positioned at the center of the atom. For calculating MEP, positive unit charge equivalent to that of a proton is placed at each grid point, and the electrostatic interaction between the atoms of the structure and the unit charge is then calculated. When calculations are completed, a map showing positive and negative isopotential contour lines is drawn. The number of grid points chosen were 15 per molecule. The levels of potential energy as defined by contour levels were +10 and -10 kcal/mol for positive and negative energy potentials, respectively.

Superdelocalizability. The superdelocalizability (S) of an atom is a measure of its available electron density. It is the ratio of orbital density to orbital energy summed over all orbitals. S is calculated from the expression (Brown and Simas, 1982; Chem-X Reference Guide, 1991, Volume II, pp 14-26)

$$S = \sum_j n_j \sum_m (C_{jm}^2 / \epsilon_j)$$

where n_j is the number of electrons in molecular orbital j , C_{jm} is the eigenvector of atomic orbital m in molecular orbital j , and ϵ_j is the eigenvalue (energy) of molecular orbital j .

The S of highest occupied molecular orbital (S_{HOMO}) and lowest unoccupied molecular orbital (S_{LUMO}) and electrophilic S (S_{E}) and nucleophilic S (S_{N}) based on occupied and unoccupied orbitals, respectively, were computed for inclusion in the QSAR analysis. The orbital energy of HOMO (ϵ_{HOMO}) and LUMO (ϵ_{LUMO}) were also included in the QSAR analysis.

RESULTS

Competitive Inhibition. In competitive binding studies, we examined whether the selected phenopylate analogues competed for binding with [^{14}C]AF for the same binding sites on Protox-containing etioplast membranes. Figure 2 shows that all five analogues tested reduced the amount of labeled AF bound to barley etioplasts by varying degrees. Also, the specific binding constants of AF in the presence of these analogues were directly related to their Protox-inhibitory abilities (Table III). In another experiment, we looked at the abilities of RH-0978 (second most inhibitory analogue in the set) and unlabeled AF to compete with [^{14}C]AF to determine the relative binding affinities of AF and RH-0978 toward Protox. We found that RH-0978 competed with [^{14}C]AF more effectively than did unlabeled AF (Figure 3), which agreed with their I_{50} values of 0.03 and 4 μM for RH-0978 and AF, respectively.

Table III. Protox I_{50} Values and Specific Binding Constants of Selected Compounds

compd	I_{50} , μM	binding constants, nM	
		expt 1	expt 2
[^{14}C]acifluorfen (AF)		41.1	28.4
[^{14}C]AF + unlabeled AF			50.5
[^{14}C]AF + RH-1908	4000	45.1	
[^{14}C]AF + RH-1909	240	49.3	
[^{14}C]AF + phenopylate	2.7	56.9	
[^{14}C]AF + RH-6251	0.28	92.5	
[^{14}C]AF + RH-0978	0.03	123.3	75.0

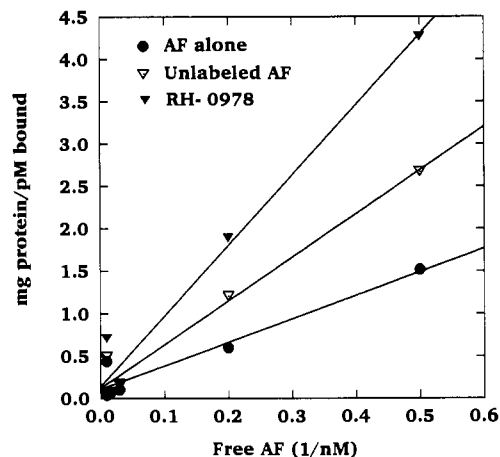


Figure 3. Binding of [^{14}C]acifluorfen (AF) in the presence of 100 nM unlabeled AF and RH-0978.

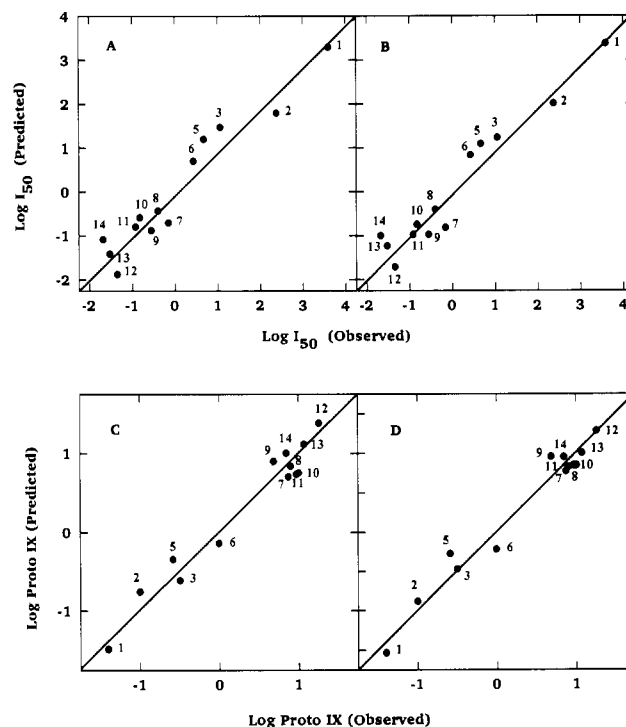


Figure 4. Plots of observed vs predicted values of $\log I_{50}$ from eqs 9 (A) and 10 (B) and of $\log \text{Proto IX}$ from eqs 11 (C) and 12 (D). Numbers correspond to compounds in Table I.

QSAR Analysis. The RSQUARE method of SAS (SAS Institute Inc., Cary, NC) was used to choose the variables for building regression models. There were 35 molecular properties (Table II) representing bulk, steric, electronic, and lipophilicity parameters considered as independent variables and three biological activities considered as dependent variables. For each biological property, this procedure identified three independent variables which singly contributed to the variation ($R^2 = 0.66-0.79$) in the

Table IV. Compounds and Their Biological and Molecular Properties Used in the Regression Equations 1-12

compd	I_{50} , ^a μM	Proto IX ^{a,b}	HA ^{a,c}	VDW _{volume} , \AA^3	S_E , eV	ϵ_{LUMO} , eV	$\log P$
RH-1908	4000	0.04	-6	151.3	-3.06	-0.08	2.73
RH-1909	240	0.10	8	161.6	-3.39	-0.43	3.13
RH-1911	11.5	0.32	40	172.8	-3.36	-0.53	3.38
RH-7160	7.5	0.24	2	225.8	-4.57	-0.91	3.95
RH-9611	4.7	0.26	-4	195.2	-3.93	-0.87	2.98
phenopylate	2.7	0.99	49	180.8	-3.68	-0.84	3.94
RH-1965	0.7	7.45	439	225.8	-4.52	-1.25	3.95
RH-1964	0.4	8.00	604	250.4	-4.92	-1.22	4.67
RH-6251	0.28	4.86	344	239.8	-4.76	-0.92	4.25
RH-0710	0.15	10.09	492	248.3	-5.07	-0.69	2.93
RH-4663	0.12	9.37	582	228.4	-4.56	-0.93	3.82
RH-1224	0.045	18.14	949	249.1	-5.26	-1.08	3.57
RH-0978	0.030	11.81	769	238.9	-5.06	-1.09	3.42
RH-1422	0.021	7.03	678	238.4	-4.85	-1.24	4.20

^a Values are from Nandihalli et al. (1992b). ^b Protoporphyrin IX content caused to accumulate by 100 μM herbicide expressed as nmol/g of fresh weight. ^c Herbicidal activity as indicated by electrolyte leakage from tissue into the external medium expressed as $\mu\text{mho cm}^{-1}$ (g of fresh weight)⁻¹. Negative values indicate leakage below the levels found in untreated control treatments.

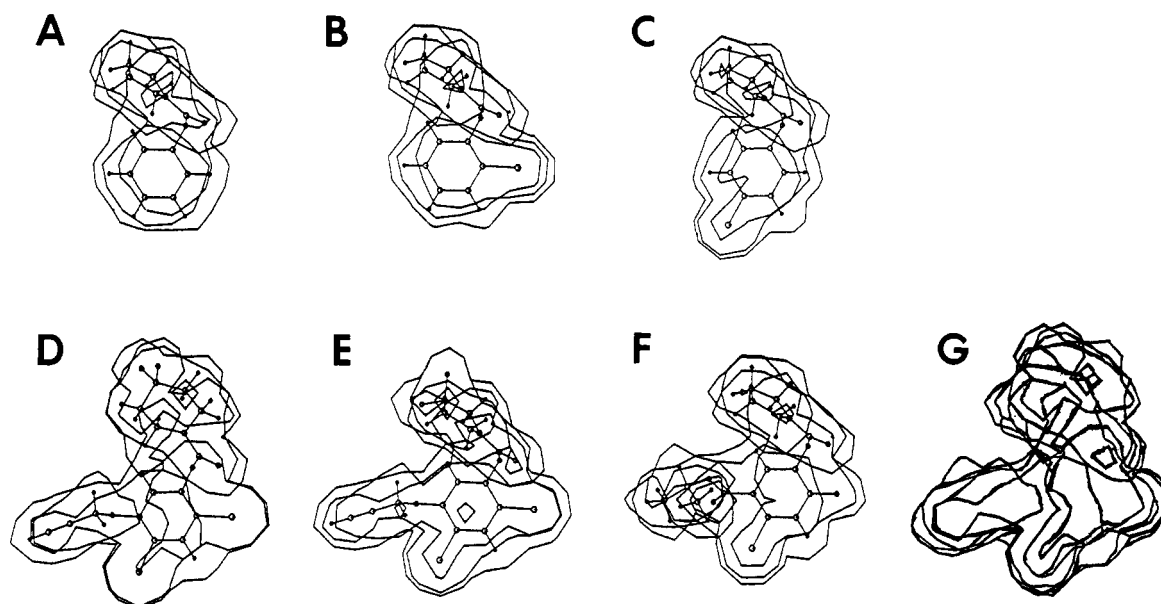


Figure 5. Three-dimensional van der Waals volume maps of least active (A, RH-1908; B, RH-1909; and C, RH-1911), most active (D, RH-1224; E, RH-0978; and F, RH-1422), and receptor-allowed maps (G) of phenopylate analogues.

dependent variables. Furthermore, the correlation coefficients (r) between the three descriptors ranged from 0.79 to 0.99. These parameters are provided in Table IV. None of the other molecular properties produced significant statistics when included in models 1-8.

$$\log I_{50} = 8.18 + 18.5 (S_E) \quad n = 14 \quad R^2 = 0.79 \quad (1)$$

$$\log I_{50} = 8.35 - 0.04 (\text{VDW}_{\text{volume}}) \quad n = 14 \quad R^2 = 0.77 \quad (2)$$

$$\log I_{50} = 3.40 + 3.80 (\epsilon_{\text{LUMO}}) \quad n = 14 \quad R^2 = 0.71 \quad (3)$$

$$\log \text{Proto IX} = -4.51 - 1.09 (S_E) \quad n = 14 \quad R^2 = 0.79 \quad (4)$$

$$\log \text{Proto IX} = -4.64 + 0.02 (\text{VDW}_{\text{volume}}) \quad n = 14 \quad R^2 = 0.79 \quad (5)$$

$$\log \text{Proto IX} = -1.56 - 2.10 (\epsilon_{\text{LUMO}}) \quad n = 14 \quad R^2 = 0.79 \quad (6)$$

$$\text{HA} = -1331.3 - 386.9 (S_E) \quad n = 14 \quad R^2 = 0.71 \quad (7)$$

$$\text{HA} = -1302.1 + 7.7 (\text{VDW}_{\text{volume}}) \quad n = 14 \quad R^2 = 0.66 \quad (8)$$

In eqs 1, 2, 4, and 5, the analogue RH-7160 (Table I) appeared consistently as an outlier in the regression analyses. Since this compound had a major structural difference (acyclic nitrogen) from the rest of the compounds, we performed regression analyses by omitting this compound. This resulted in the appearance of $\log P$ in the models with a significant improvement in R^2 values.

$$\log I_{50} = 26.29 + 1.67 (S_E) - 10.19 (\log P) + 1.33 (\log P)^2 \quad n = 13 \quad R^2 = 0.93 \quad (9)$$

$$\log I_{50} = 28.92 - 0.037 (\text{VDW}_{\text{volume}}) - 11.56 (\log P) + 1.55 (\log P)^2 \quad n = 13 \quad R^2 = 0.94 \quad (10)$$

$$\log \text{Proto IX} = -11.54 - 1.01 (S_E) + 3.92 (\log P) - 0.50 (\log P)^2 \quad n = 13 \quad R^2 = 0.96 \quad (11)$$

$$\log \text{Proto IX} = -13.13 + 0.02 (\text{VDW}_{\text{volume}}) + 4.74 (\log P) - 0.63 (\log P)^2 \quad n = 13 \quad R^2 = 0.97 \quad (12)$$

Figure 4 shows a graph of observed vs predicted values of I_{50} and Proto IX as derived from eqs 9-12. The predicted I_{50} values of RH-1908 and RH-1909 deviated greatly from the observed values, because of their highest observed I_{50} in the set. The equations comprising $\text{VDW}_{\text{volume}}$ (eqs 10

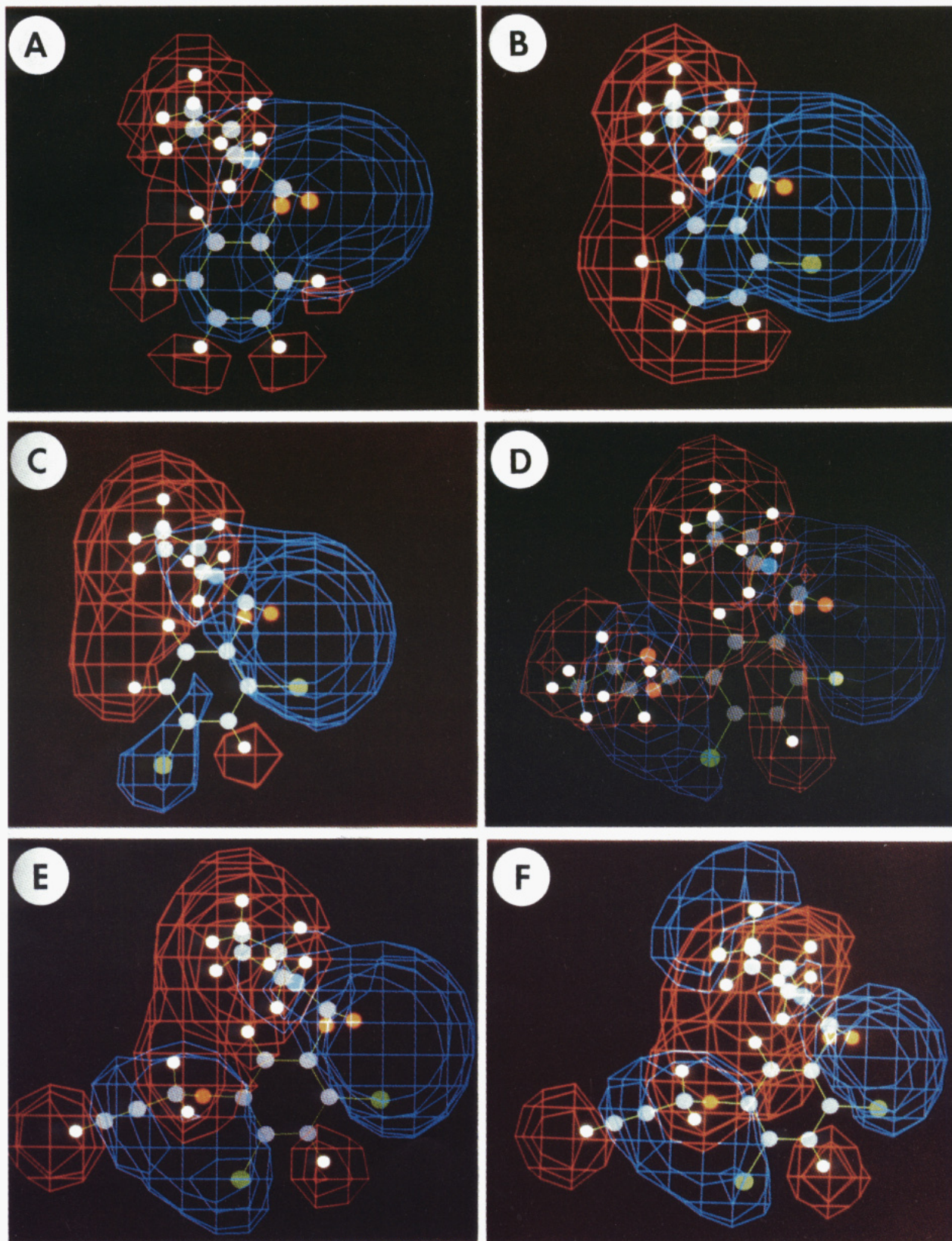


Figure 6. Electrostatic potential maps, derived from atomic point charges, of (A) RH-1908, (B) RH-1909, (C) phenopylate, (D) RH-1422, (E) RH-4663, and (F) RH-0978 showing distribution of negative (blue) and positive (red) electrostatic isopotential contours at an energy level of 10 kcal/mol for positive potential and -10 kcal/mol for negative potential. Color coding for atoms: carbon, large white; hydrogen, small white; nitrogen, blue; oxygen, orange; chlorine, green; fluorine, light green.

and 12) predicted I_{50} and Proto IX values better than the equations with S_E , even though these equations had similar R^2 values.

From the regression models above and Tables IV, clearly the VDW_{volume} of herbicides positively correlated with their capacity to inhibit Protox, induce Proto IX accumulation,

and cause herbicidal injury. Furthermore, the herbicides that showed greatest effects on the biological activities had VDW_{volume} greater than 225 \AA^3 (Table IV). Figure 5 shows the 3D graphical presentation of VDW_{volume} of the three least active (A–C) and the three most active (D–F) compounds. Clearly, the active and inactive molecules

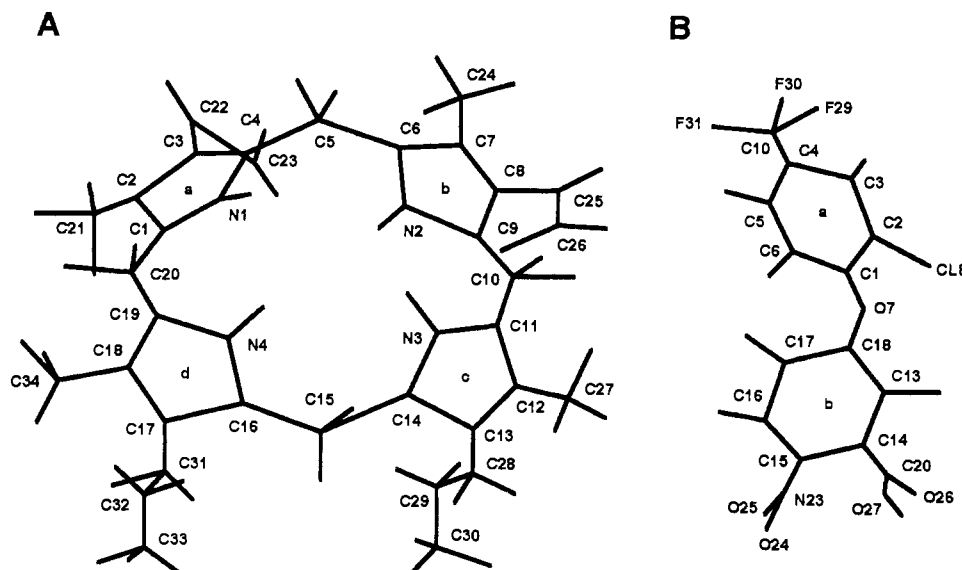


Figure 7. Three-dimensional optimized structures of (A) Protogen and (B) acifluorfen. Hydrogen atoms are not labeled.

differed in their shapes primarily around the phenyl ring. It is well-known that all active molecules must fit the receptor, and therefore, any volume occupied by an active molecule must fit into an empty space in the receptor. Figure 5G is the combined VDW_{volume} map of the aforementioned three most active analogues. In this figure, the VDW_{volume} maps of individual structures are overlaid corresponding to their common fitted structures. Assuming that these conformers represent the actual conformers at the active site, the map in Figure 5G represents a likely receptor-allowed shape.

The relationships between the two electronic parameters, S_E and ϵ_{LUMO} , and the biological activities were also linear, with more negative values associated with higher activities (Table IV). Equations 9–12 indicated that the relationships between the lipophilicity parameter, $\log P$, and biological activities were curvilinear.

Comparative Analysis of Molecular Electrostatic Potentials. Qualitative analysis of negative and positive potentials as to their distribution around the structures clearly revealed definite trends between MEP distribution patterns and enzyme inhibitory activity (I_{50}). For example, in RH-1908 (the least active compound in the set) the negative MEP (–MEP) is located on one side of the molecule as a single field (Figure 6A). Although RH-1909 (the next least active compound) had slightly stronger –MEP (281.8 Å³) than the most active compound RH-1422 (233.8 Å³), its –MEP distribution pattern is similar to that of RH-1908 (Figure 6B). The phenopylate compound which was about 1480-fold more active than the least active compound has a distinct, but much smaller, second–MEP field (Figure 6C). In RH-1422 the –MEP is at two locations, opposite each other, one associated with the F/COO–N region and the other surrounding the Cl/COO region of the molecule (Figure 6D). In RH-1908, RH-1909, and phenopylate the positive MEP (+MEP) is present mainly as one large area, but in RH-1422 it is present as three fields. RH-0978 having F₂ substitution on the pyrrolidine ring showed a third –MEP field as compared to RH-4663, which was 4 times less active than RH-0978 (Figure 6E,F). The electrostatic fields were not significantly altered by substituting a piperidine ring for a pyrrolidine ring (maps not shown).

The –MEP regions actually extend over the phenyl rings in RH-1908 and RH-1909 molecules (Figure 6A,B). This is a characteristic feature of aromatic rings that is attributed to the π electrons of the ring. This –MEP region

is weakened or eliminated upon the introduction of one or more electron-withdrawing groups such as Cl, F, and CO₂R as shown in Figure 6C–F. These electron-withdrawing groups have characteristic negative regions associated with them, even when substituted on the five-membered alicyclic ring (Figure 6F).

DISCUSSION

In the competitive type of enzyme inhibition, the inhibitor resembles the substrate closely and binds to the active site of the enzyme. It has been shown that AF competitively binds to Protox with respect to its substrate Protogen (Matringe et al., 1989a). Furthermore, three other structurally unrelated compounds reduced the specific binding constant of AF, suggesting that these structures share common sites on the enzyme (Varsano et al., 1990). In the present study, we have shown that five phenopylate analogues competed with the [¹⁴C]AF for sites on Protox-containing barley etioplast membrane preparations. The extent of competition was affected by structural variations and was directly related to their enzyme-inhibitory activity. In our earlier modeling study (Nandihalli et al., 1992a), we showed that, sterically, AF represented half the fraction of Protogen molecule (Figure 7). A close steric resemblance exists between AF and the 10 most active phenopylate analogues used in this study. The van der Waals volume of AF and the average volume of the 10 most active phenopylate analogues were 226 and 229 Å³, respectively. Furthermore, the negative electrostatic potential volumes of AF and the average potentials of the same 10 phenopylate analogues were 213.6 and 219.7 Å³, respectively. There were also qualitative similarities between AF and these active analogues with respect to negative electrostatic potential distribution patterns.

Varsano et al. (1990) reported a specific binding constant (K) of 13.6 ± 4.1 nM for [³H]AF using corn etioplast membranes. The K was much lower than the inhibition constant of 120 nM for AF (Camadro et al., 1991). These values are usually close to each other. In our study with barley etioplast membranes, the K for [¹⁴C]AF ranged from 28.4 to 41.1 nM (Table III). This discrepancy between our K values and that of Varsano et al. (1990) may be due to differences in plant species and plastid isolation methods used. Furthermore, the variation in the K of AF between experiments 1 and 2 was probably due to the very low specific activity of [¹⁴C]AF used and the use of two

different etioplast preparations from plants grown at different times. However, the trends in K values remained the same (compare K values of RH-0978 in experiments 1 and 2 with that of AF only in Table III).

To be effective, a bioactive substance must reach the active site and have high binding affinity toward the enzyme. $\log P$, an indicator of a molecule's lipophilicity, has been used in QSAR studies to represent a transport parameter of bioactive substances. $\log P$ indicates the ability of a chemical to move through the biomembranes to reach the active site. The fact that the lipophilicity was one of the factors that appeared in regression models, relating Prottox I_{50} to molecular properties, suggests that the active site of Prottox enzyme is embedded in the cell membranes. Furthermore, the relationships between $\log P$ and biological activities were curvilinear. In general, the rate of barrier crossing increases with the value of $\log P$ up to the point that molecules become so large that their diffusion coefficients start to decrease because of their increased interaction with membrane lipids (Leo et al., 1971). Thus, it is common to expect a parabolic dependence of biological properties on $\log P$ as presented in eqs 9–12 of this work.

The electrophilic superdelocalizability (S_E) and energy of LUMO of phenopylate analogues negatively correlated with their biological activities (Table IV). S has been found to be a predictor in the regression models of the inhibitors of the porphyrin pathway (Nandihalli and Rebeiz, 1991), Prottox inhibitors (Nandihalli et al., 1992a), and plant growth regulators (Fukui et al., 1958). Fukui et al. (1958) found a positive correlation between the S_{LUMO} of the *o*-carbon of the benzene ring and plant growth activity of a number of benzoic acid derivatives.

MEP is a molecular property which is used in the study of biological recognition processes and molecular reactivity. An understanding of the MEP distribution patterns of active analogues provides insights into the nature of interaction of inhibitors with the receptor (Murray et al., 1986). In the present study, a comparative analysis of MEP patterns of analogues indicated that for high biological activity the analogues should have at least two -MEP fields located approximately opposite to each other (Figure 6D). Furthermore, we suggest that these negative potentials appear to be the major regions through which the herbicide molecules interact with the binding sites of the enzyme. The negative potentials tend to attract an approaching electrophile including a proton donor in a hydrogen bond (Murray et al., 1991). Therefore, in highly active analogues with two carbonyl groups or a carbonyl and a propargyl ether group, located opposite each other, it is likely that hydrogen bonding with the active site is involved.

On the basis of the research and from our earlier QSAR study of diphenyl ether analogues (Nandihalli et al., 1992a), we suggest that the Prottox inhibitors must contain at least two aromatic or alicyclic rings, mainly to satisfy the geometric requirement of a half portion of the Protogen molecule (two adjacent pyrrole rings, Figure 7). Second, one of the rings (phenyl ring in both classes) must have substitutions such that they expand molecular bulk as well as create at least two negative electrostatic potential fields around this phenyl ring. To date, at least 10 different chemical classes have been known to inhibit Prottox activity and all are bicyclic. Our future research will attempt to determine the molecular commonalities between these different chemical classes of Prottox inhibitors.

ACKNOWLEDGMENT

We gratefully acknowledge Dr. Alfred French of USDA-ARS, SRRC, New Orleans, for his advice and for providing

us with molecular modeling facilities. We thank Dr. Colin M. Tice of Rohm and Haas Co. for his invaluable assistance in providing technical grade herbicides, advice, and constructive criticism and BASF Co. for supplying [14 C]acifluorfen. We also thank Drs. Robert D. Clark and Jane S. Murray of Monsanto Co. and Chemistry Department, University of New Orleans, respectively, for their constructive criticisms and suggestions.

LITERATURE CITED

- Becerril, J. M.; Duke, S. O. Protoporphyrin IX content correlates with activity of photobleaching herbicides. *Plant Physiol.* **1989**, *90*, 1175–1181.
- Brown, R. E.; Simas, A. M. On the applicability of CNDO indices for the prediction of chemical reactivity. *Theor. Chim. Acta* **1982**, *62*, 1–16.
- Camadro, J. M.; Urban-Grimal, D.; Labbe, P. A new assay of protoporphyrinogen oxidase—Evidence for a total deficiency in that activity in a heme-less mutant of *Saccharomyces cerevisiae*. *Biochem. Biophys. Res. Commun.* **1982**, *106*, 724–730.
- Camadro, J. M.; Matringe, M.; Scalla, R.; Labbe, P. Kinetic studies on protoporphyrinogen oxidase by diphenyl ether herbicides. *Biochem. J.* **1991**, *277*, 17–21.
- Deybach, J. C.; de Verneuil, H.; Nordmann, Y. The inherited enzymatic defect in porphyria variegata. *Hum. Genet.* **1981**, *58*, 425–428.
- Duke, S. O.; Becerril, J. M.; Sherman, T. D.; Lydon, J.; Matsumoto, H. The role of protoporphyrin IX in the mechanism of action of diphenyl ether herbicides. *Pestic. Sci.* **1990**, *30*, 367–378.
- Duke, S. O.; Becerril, J. M.; Sherman, T. D.; Matsumoto, H. Photosensitizing porphyrins as herbicides. *Am. Chem. Soc. Symp. Ser.* **1991**, No. 449, 371–386.
- Ellgehasen, H.; D'Hondt, C.; Fuerer, R. Reversed-phase chromatography as a general method for determining octan-1-ol/water partition coefficients. *Pestic. Sci.* **1981**, *12*, 219–227.
- Fukui, K.; Nagata, C.; Yonezawa, T. Electronic structure and auxin activity of benzoic acid derivatives. *J. Am. Chem. Soc.* **1958**, *80*, 2267–2270.
- Jacobs, J. M.; Jacobs, N. J.; Borotz, S. E.; Guerinot, M. L. Effects of the photobleaching herbicide, acifluorfen-methyl, on protoporphyrinogen oxidation in barley organelles, soybean root mitochondria, soybean root nodules, and bacteria. *Arch. Biochem. Biophys.* **1990**, *280*, 369–375.
- Jacobs, J. M.; Jacobs, N. J.; Sherman, T. D.; Duke, S. O. Effect of diphenyl ether herbicides on oxidation of protoporphyrinogen to protoporphyrin in organellar and plasma membrane enriched fractions of barley. *Plant Physiol.* **1991**, *97*, 197–203.
- Lehnen, L. P.; Sherman, T. D.; Becerril, J. M.; Duke, S. O. Tissue and cellular localization of acifluorfen-induced porphyrins in cucumber cotyledons. *Pestic. Biochem. Physiol.* **1990**, *37*, 239–248.
- Leo, A.; Hansch, C.; Elkins, D. Partition coefficients and their uses. *Chem. Rev.* **1971**, *71*, 525–616.
- Lydon, J.; Duke, S. O. Porphyrin synthesis is required for photobleaching activity of the *p*-nitrosubstituted diphenyl ether herbicides. *Pestic. Biochem. Physiol.* **1988**, *31*, 74–83.
- Matringe, M.; Scalla, R. Studies on the mode of action of acifluorfen-methyl in non-chlorophyllous soybean cells: Accumulation of tetrapyrroles. *Plant Physiol.* **1988a**, *86*, 619–622.
- Matringe, M.; Scalla, R. Effects of acifluorfen-methyl on cucumber cotyledons: Protoporphyrin accumulation. *Pestic. Biochem. Physiol.* **1988b**, *32*, 164–172.
- Matringe, M.; Camadro, J. M.; Labbe, P.; Scalla, R. Protoporphyrinogen oxidase as a molecular target for diphenyl ether herbicides. *Biochem. J.* **1989a**, *260*, 231–235.
- Matringe, M.; Camadro, J. M.; Labbe, P.; Scalla, R. Protoporphyrinogen oxidase inhibition by three peroxidizing herbicides: oxadiazon, LS 82-556 and M & B 39279. *FEBS Lett.* **1989b**, *245*, 35–38.
- Matsumoto, H.; Duke, S. O. Acifluorfen-methyl effects on porphyrin synthesis in *Lemna paucicostata* Hegelm. 6746. *J. Agric. Food Chem.* **1990**, *38*, 2066–2071.

- Murray, J. S.; Zilles, B. A.; Jayasuriya, K.; Politzer, P. Comparative analysis of electrostatic potentials of dibenzofuran and some dibenzo-*p*-dioxins. *J. Am. Chem. Soc.* **1986**, *108*, 915-918.
- Murray, J. S.; Ranganathan, S.; Politer, P. Correlations between the solvent hydrogen bond acceptor parameter β and the calculated molecular electrostatic potentials. *J. Org. Chem.* **1991**, *56*, 3734-3737.
- Nandihalli, U. B.; Rebeiz, C. A. Photodynamic herbicides 9. Structure activity study of substituted 1,10-phenanthrolines as potent photodynamic herbicide modulators. *Pestic. Biochem. Physiol.* **1991**, *40*, 27-46.
- Nandihalli, U. B.; Liebl, R. A.; Rebeiz, C. A. Photodynamic herbicides VIII. Mandatory requirement of light for the induction of protoporphyrin IX accumulation in acifluorfen-treated cucumber. *Pestic. Sci.* **1991**, *31*, 9-23.
- Nandihalli, U. B.; Duke, M. V.; Duke, S. O. Quantitative structure-activity relationships of protoporphyrinogen oxidase-inhibiting diphenyl ether herbicides. *Pestic. Biochem. Physiol.* **1992a**, *43*, 193-211.
- Nandihalli, U. B.; Sherman, T. D.; Duke, M. V.; Fischer, J. D.; Musco, V. A.; Becerril, J. M.; Duke, S. O. Protoporphyrinogen oxidase inhibition by *O*-phenyl pyrrolidino- and piperidino-carbamates correlates with herbicidal effects. *Pestic. Sci.* **1992b**, in press.
- Nicolaus, B.; Sandmann, G.; Watanabe, H.; Wakabayashi, K.; Böger, P. Herbicide-induced peroxidation: Influence of light and diuron on protoporphyrin IX formation. *Pestic. Biochem. Physiol.* **1989**, *35*, 192-201.
- Sherman, T. D.; Duke, M. V.; Clark, R. D.; Sanders, E. F.; Matsumoto, H.; Duke, S. O. Pyrazole phenyl ether herbicides inhibit protoporphyrinogen oxidase. *Pestic. Biochem. Physiol.* **1991a**, *40*, 236-245.
- Sherman, T. D.; Becerril, J. M.; Matsumoto, H.; Duke, M. V.; Jacobs, J. M.; Jacobs, N. J.; Duke, S. O. Physiological basis for differential sensitivities of plant species to protoporphyrinogen oxidase-inhibiting herbicides. *Plant Physiol.* **1991b**, *97*, 280-287.
- Tischer, W.; Strotmann, H. Relationship between inhibitor binding by chloroplasts and inhibition of photosynthetic electron transport. *Biochim. Biophys. Acta* **1977**, *460*, 113-125.
- Varsano, R.; Matringe, M.; Magnin, N.; Mornet, R.; Scalla, R. Competitive interaction of three peroxidizing herbicides with the binding of ^3H -acifluorfen to corn etioplast membranes. *FEBS Lett.* **1990**, *272*, 106-108.
- Witkowski, D. A.; Halling, B. P. Accumulation of photodynamic tetrapyrroles induced by acifluorfen-methyl. *Plant Physiol.* **1988**, *87*, 632-637.
- Witkowski, D. A.; Halling, B. P. Inhibition of plant protoporphyrinogen oxidase by the herbicide acifluorfen-methyl. *Plant Physiol.* **1989**, *90*, 1239-1242.

Received for review March 5, 1992. Revised manuscript received June 22, 1992. Accepted July 6, 1992.

Registry No. 1, 55379-71-0; 2, 143121-06-6; 3, 1759-02-0; 4, 143121-07-7; 5, 143121-08-8; 6, 40575-34-6; 7, 133636-94-9; 8, 133636-96-1; 9, 87374-78-5; 10, 143121-09-9; 11, 87365-63-7; 12, 138926-22-4; 13, 143121-10-2; 14, 133636-98-3; protoporphyrinogen oxidase, 53986-32-6; protoporphyrinogen IX, 7412-77-3.